# Modulating the Midpoint Potential of the [4Fe-4S] Cluster of the Nitrogenase Fe Protein[†,‡]

Se Bok Jang, Lance C. Seefeldt, and John W. Peters*

*Department of Chemistry and Biochemistry, Utah State University, Logan, Utah 84322*

*Received July 22, 1999; Revised Manuscript Received November 3, 1999*

ABSTRACT: Protein-bound [FeS] clusters function widely in biological electron-transfer reactions, where their midpoint potentials control both the kinetics and thermodynamics of these reactions. The polarity of the protein environment around [FeS] clusters appears to contribute largely to modulating their midpoint potentials, with local protein dipoles and water dipoles largely defining the polarity. The function of the [4Fe-4S] cluster containing Fe protein in nitrogenase catalysis is, at least in part, to serve as the nucleotide-dependent electron donor to the MoFe protein which contains the sites for substrate binding and reduction. The ability of the Fe protein to function in this manner is dependent on its ability to adopt the appropriate conformation for productive interaction with the MoFe protein and on its ability to change redox potentials to provide the driving force required for electron transfer. Phenylalanine at position 135 is located near the [4Fe-4S] cluster of nitrogenase Fe protein and has been suggested by amino acid substitution studies to participate in defining both the midpoint potential and the nucleotide-induced changes in the [4Fe-4S] cluster. In the present study, the crystal structure of the *Azotobacter vinelandii* nitrogenase Fe protein variant having phenylalanine at position 135 substituted by tryptophan has been determined by X-ray diffraction methods and refined to 2.4 Å resolution. A comparison of available Fe protein structures not only provides a structural basis for the more positive midpoint potential observed in the tryptophan substituted variant but also suggests a possible general mechanism by which the midpoint potential could be controlled by nucleotide interactions and nitrogenase complex formation.

A broad range of proteins contain [FeS] clusters, the majority of which have been shown to function in electron transfer. The midpoint potential of these [FeS] clusters controls both the thermodynamics and kinetics of the electron-transfer reactions. Therefore, understanding the elements of the protein environment that dictate the properties of the bound [FeS] cluster is of significant fundamental importance (*1*, *2*). Unique to this class of proteins is the nitrogenase Fe protein in which the magnitude of the midpoint potential can be controlled through conformation states of the protein dictated by its interaction with nucleotides and its specific electron acceptor.

During the biological conversion of nitrogen to ammonia, the nitrogenase Fe protein participates as the exclusive electron donor to the MoFe protein where substrate reduction occurs (recently reviewed in refs *3*−*8*). The electron-transfer process that leads to substrate reduction on the MoFe protein involves the hydrolysis of MgATP, which occurs on the Fe protein within the nitrogenase Fe protein−MoFe protein complex. The X-ray crystal structures of the Fe protein and the MoFe protein have been determined from *Azotobacter vinelandii* and *Clostridium pasteurianum* (*9*−*15*). The nitrogenase Fe protein exists as a dimer of identical subunits bridged by a single [4Fe-4S] cubane. The MoFe protein is an $\alpha_2\beta_2$-tetramer that contains two types of metalloclusters, the FeMo cofactor, and the P cluster. Each $\alpha\beta$-dimer is thought to function as an independent half and contains one FeMo cofactor and one P cluster. The FeMo cofactor (1Mo-7Fe-9S-homocitrate) is located entirely within the α-subunit and is the site of substrate binding and reduction (*16*). The P cluster is located at the interface of the α- and $\beta$-subunits, and it is believed to participate in the transfer of electrons from the Fe protein to the substrate reduction site (*17*−*21*). During catalysis, the Fe protein dimer docks with the MoFe protein such that the 2-fold symmetric axis of the Fe protein pairs with the pseudo symmetric $\alpha\beta$-subunit interface of the MoFe protein to form a complex placing the [4Fe-4S] cluster of the Fe protein in close proximity to the P cluster of the MoFe protein for intermolecular electron transfer. The reduction of a single molecule of dinitrogen requires multiple electron transfer events, and dissociation of the complex likely represents the rate-limiting step during turnover (*22*).

Both structural (*23*) and amino acid sequence comparisons (*24*) indicate the Fe protein is a member of a large class of proteins that couple the energy from the binding and hydrolysis of nucleotide triphosphates to changes in protein conformation. In the nitrogenase system, these conformational changes result in productive Fe protein−MoFe protein complex formation leading to electron transfer from the [4Fe-4S] cluster of the Fe protein to the substrate reduction site of the MoFe protein. It has been demonstrated previously

[†] This work was supported by United States Department of Agriculture Grant 9803559 (to J.W.P.) and National Science Foundation Grant MCB-9722937 (to L.C.S.).

[‡] Atomic coordinates have been submitted to the Brookhaven Protein Data Bank, code 1de0.

* To whom correspondence should be addressed. Phone: (435) 797-1609. Fax: (435) 797-3390. E-mail: petersj@cc.usu.edu.

10.1021/bi991694v CCC: $19.00 
Published on Web 01/08/2000

that nucleotide binding and subsequent Fe protein−MoFe protein complex formation results in negative shifts in the midpoint potential of the [4Fe-4S] cluster of the Fe protein (*25*−*28*), increasing the driving force for electron transfer to substrate reduction. Nucleotide binding causes changes in the midpoint potential (*25*−*28*) and other biophysical properties (*25*, *29*−*33*) of the [4Fe-4S] of the Fe protein presumably by remotely triggering changes in the protein environment around the cluster. Examination of the three-dimensional structures of proteins containing [4Fe-4S] clusters has suggested that the polarity around the [4Fe-4S] clusters of these proteins contributes to defining the midpoint potential of the cluster (*1*, *2*, *34*−*38*). Some important factors in defining the polarity of the cluster environment are solvent accessibility, proximity of main-chain amide dipoles, and the composition of amino acid side chains in the environment.

From the X-ray crystal structure of the *A. vinelandii* native Fe protein, several amino acid residues can be identified in the environment of the [4Fe-4S] cluster that could influence the local charge and the solvent accessibility (*9*, *15*). One notable residue, phenylalanine 135, is located such that the atoms of the benzene ring of this residue in each monomer approach van der Waals distance of inorganic S atoms of the [4Fe-4S] cluster. Mutagenesis studies have revealed that the conserved Phe at position 135 in the nitrogenase Fe protein of *A. vinelandii* plays an important role in defining several biochemical and biophysical properties of the [4Fe-4S] cluster (*39*). Substitution of Phe 135 by either Tyr, Ile, His, or Trp result in Fe proteins that are no longer competent for MgATP hydrolysis or electron transfer to the MoFe protein. Significantly, all of these substitutions influence the midpoint potential of the $[4Fe\text{-}4S]^{2+/1+}$ couple in the nucleotide-free and nucleotide-bound forms of the Fe protein. For example, the midpoint potential of the [4Fe-4S] cluster of the Trp substituted variant is found to be −230 mV in the nucleotide-free form in contrast to the native Fe protein which has a corresponding midpoint potential of −310 mV in this state.

To further understand the role of Phe 135 in Fe protein function and nitrogenase catalysis, we have determined the X-ray crystal structure of the nitrogenase Fe protein with Phe at position 135 substituted by Trp in its nucleotide-free form. The results establish a structural basis for the changes in midpoint potential of the [4Fe-4S] cluster. Comparisons of available Fe protein structures allow consideration of factors that contribute to coupling protein conformational changes in the [4Fe-4S] cluster environment with defined changes in the midpoint potential of the cluster.

## EXPERIMENTAL PROCEDURES

Expression and purification of altered Fe protein were accomplished as previously described (*39*). The Fe protein was purified in 50 mM Tris buffer, pH 8.0, in the presence of 2 mM sodium dithionite, and included 20% glycerol as a stabilizing agent. Protein concentrations were determined by a modified biuret method (*40*) using bovine serum albumin as the standard. The protein was homogeneous as determined by SDS gels stained with Coomassie blue (*41*). Protein was protected from oxygen by manipulation in sealed serum vials with 2 mM dithionite or in an argon atmosphere glovebox (Vacuum Atmospheres, Hawthorne, CA) with less than 0.5 ppm oxygen.

Table 1: Data and Refinement Statistics[a]

| | |
|---|---|
| space group | $P2_1$ |
| cell dimensions | |
| *a* (Å) | 56.54 |
| *b* (Å) | 91.05 |
| *c* (Å) | 63.35 |
| $\beta$ (deg) | 99.76 |
| resolution (Å) | 20.0−2.4 |
| completeness (%) (2.44−2.40) Å | 95.2 (75.5) |
| observed reflections | 265 157 |
| unigue reflections | 24 852 |
| $I/\sigma$ | 18.4 (3.9) |
| $R_{merge}$(%)[b] | 7.7 (25.3) |
| protein nonhydrogen atoms | 4380 |
| solvent molecules | 179 |
| $R_{cryst}$(%)[c] | 22.6 |
| $R_{free}$(%)[c] | 28.3 |
| bond lengths (Å) | 0.010 |
| bond angles (deg) | 2.576 |
| average <*B*> factor (Å$^2$) | 50.3 |

[a] Numbers in parentheses indicate values for the highest resolution bin. [b] $R_{merge} = \Sigma_{hkl}\Sigma_i|I_i - \langle I\rangle|/\Sigma_{hkl}\Sigma_i|\langle I\rangle|$, where $I_i$ is the intensity for the *i*th measurement of an equivalent reflection with indices *h*, *k*, *l*. [c] $R_{cryst} = \Sigma_{hkl}||F_{obs}| - |F_{calc}||/\Sigma_{hkl}|F_{obs}|$, where $F_{obs}$ denotes the observed structure factor amplitude, and $F_{calc}$ denotes the structure factor amplitude calculated from the model; 5% of reflections were used to calculate $R_{free}$ (data 20.0−2.4 Å used in the refinement).

The Fe protein was crystallized by microcapillary batch diffusion (*9*) using 30% PEG 4000, 0.1 M Tris HCl, pH 8.5, and 0.2 M sodium acetate as precipitating solution. The Fe protein crystals are dark brown in color and grow in 7 days to an average size of 0.2 × 0.3 × 0.7 mm$^3$ in space group $P2_1$ with unit cell parameters (Table 1) similar to those described previously for the native Fe protein (*9*). For data collection, the crystals were equilibrated in a mother liquor solution containing 30% glycerol, 30% PEG 4000, 0.1 M Tris, pH 8.5, and 0.2 M sodium acetate overnight. The crystals were flash cooled in liquid nitrogen on rayon loops, and data were collected under a continuous nitrogen stream at approximately 100 K. X-ray data were collected on a Rigaku R-axis IIC imaging plate system using CuK$\alpha$ radiation ($\lambda$ = 1.5418 Å) and $\phi$ scans with a scan width of 2.0°. The data were processed using DENZO and SCALEPACK (*42*). The crystals belong to the monoclinic space group $P2_1$ ($a$ = 56.54 Å, $b$ = 91.05 Å, $c$ = 63.35 Å, and $\beta$ = 99.76°), with one dimer in the asymmetric unit (60 K). A total of 265 157 reflections were measured, which reduced to 24 852 unique reflections representing 95.2% of a complete 2.4 Å data set (Table 1).

The structure was determined by the molecular replacement method by AMORE (*43*) using the Fe protein model 1nip as a search model (*9*). The search was carried out with the data between 15.0 and 4.0 Å, and since the cell parameters were very similar to that observed in the 1nip structure, solution required very little rotational and translational movement and resulted in a correlation coefficient of 69.4% and an *R*-factor of 36.2%. Solvent flattening and 2-fold noncrystallographic averaging with SOLOMON (*44*) were employed to improve map quality. The model was improved through iterative model building using the program O (*45*). During refinement, a bulk solvent correction allowed the inclusion of low-resolution reflections and ∼5% of the data were randomly selected for cross-validation (*46*). Model bias was removed for the incorporation of $R_{free}$ calculation for cross-validation by randomization using the

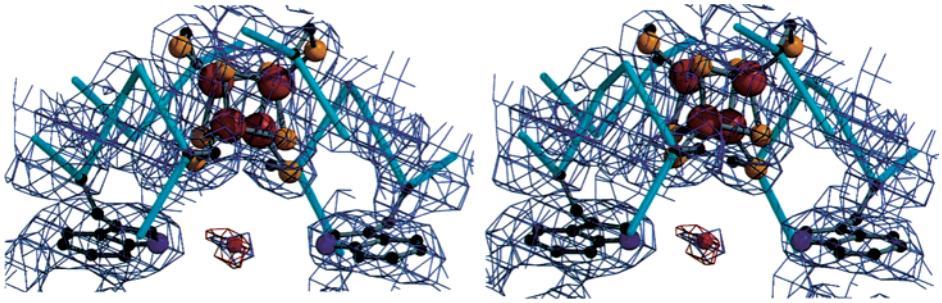

FIGURE 1: Electron density maps of the environment of the Trp 135 substitution and the [4Fe-4S] cluster of the Fe protein (stereoview). The position of Trp135 with respect to the [4Fe-4S] cluster and associated Cys ligands is represented in a ball-and-stick diagram with rust indicating Fe, yellow indicating S, blue indicating N, black indicating C, and red indicating the O of a water molecule. In navy are $2F_o - F_c$ electron density maps contoured at $1\sigma$ and in red $F_o - F_c$ electron with solvent omitted contoured at $3\sigma$.

simulated annealing routine of X-PLOR (*47*) with an annealing temperature of 4000 K. The noncrystallographic symmetry is exploited during refinement by restraining chemically identical chains to an overall rms deviation of corresponding Cα atoms of 0.45 Å (*48*). Initial positional refinement of the rigid-body-refined model using 20.0−2.4 Å data followed by group *B*-factor refinement dropped the $R_{free}$ to 30.0%. The final model has been refined to 2.4 Å resolution to a current $R_{cryst}$ of 22.6% and $R_{free}$ of 28.37% and consists of all 578 possible protein residues, one [4Fe-4S] cluster, and 224 water molecules (Table 1). The model obeys good geometry, with rms deviations from ideality for bond lengths and angles of 0.010 Å and 2.576°, respectively, and has 100% of amino acid residues in allowed regions of a Ramachandran plot (*49*). The structural representations in Figures1−3 were generated in MOLSCRIPT (*50*), BOBSCRIPT (*51*), and RASTER3D (*52*).

## RESULTS

*Overall Structure.* The structure of the altered nitrogenase Fe protein with Phe substituted by Trp has been refined to 2.4 Å resolution (Table 1). The structure reveals that, with respect to the overall conformation of the previously characterized Fe protein structures, the Trp-substituted protein is largely unchanged, indicating that the changes in biochemical and biophysical properties of the [4Fe-4S] are likely due to changes in its local environment only. The structures were compared by first a superposition (*48*) of the dimers of each Fe protein structure followed by the same treatment using individual monomers. Very little difference in the overall rms deviations (0.75 Å for the individual monomers versus 0.79 Å for the dimers using 1nip for the superposition) in the two scenarios indicates the Trp substitution has not resulted in a significant rigid body repositioning of the monomers with respect to one another.

*Environments of the Substitution and Fe−S Cluster.* Density for the Trp residue was very clear in electron density maps revealing the position and orientation of the Trp side chain (Figure 1). The orientation of the Trp indole side chain indicates that the amide nitrogen of the indole moiety of each Trp is located in close proximity to the [4Fe-4S] cluster approaching within ∼4.4 Å of S atoms of the cluster cubane. A water molecule is found to be asymmetrically coordinated by the Trp amide dipoles and located within hydrogen bond distance of the S of the [4Fe-4S] cubane (Figure 1).

The site of the substitution at position 135 is very close to the Cys 132 coordinating ligands of the [4Fe-4S] cluster. It has been inferred by amino acid substitution studies that MgATP-dependent signal transduction occurs through a pathway involving the Asp residues at position 125 (*53*) through the main chain (*54*) to the Cys 132 coordinating ligands.

Refinement of the Fe protein variant presented here was accomplished in the presence of NCS restraints applied using X-PLOR (*47*) resulting in rms deviations of ∼0.15 Å for the symmetry-related monomers. Careful inspection of electron density maps indicated no noticeable deviations from NCS that were not represented in the final model, and a good quality of fit of the data to the final model refined in this manner was observed. Table 2 shows a comparison of the distances of amide N atoms to the S atoms of the [4Fe-4S] cluster and its coordinating ligands of the Trp-substituted Fe protein variant, the native Fe protein structures, 1nip (*9*) and 2nip (*15*), and the Fe protein of the Fe protein−MoFe protein nitrogenase complex stabilized with tetraflouoaluminate and MgADP (*21*). The helices which span residues 98−122 and 133−141 are both directed at the [4Fe-4S] cluster in the native Fe protein structure. These helices are directed at the [4Fe-4S] cluster to a much lesser extent in the Fe protein from the structure of the nitrogenase complex stabilized by MgADP and tetraflouroaluminate.

In comparison of the native Fe protein to the Trp-substituted variant, the majority of distances remains similar; however, the substitution has resulted in changes in the main chain that bring the peptide bond amide of residue 135 greater than 0.5 Å closer to the S atom of Cys 132 to within ∼3.6 Å. In addition, the mutation introduces an amide from the side chain which is located ∼4.4 Å from the cluster S atoms.

## DISCUSSION

*Protein Control of the Midpoint Potential of the [4Fe-4S] Cluster.* Changing Phe 135 to Trp results in a +90 mV change in the midpoint potential of the $[4Fe\text{-}4S]^{2+/1+}$ cluster (*39*). Examination of the structure of the Trp 135 altered Fe protein presented here provides the opportunity to define how the Fe protein controls the midpoint potential of the [4Fe-4S] cluster. In addition, these observations may impact our broader understanding of protein control of the electronic properties of Fe−S clusters. The presence of the larger Trp side chain at position 135 at the interface of the homodimers of the Fe protein did not result in significant differences in the relationship of one monomer to another indicated by the superposition of the carbon α atoms of the amino acid

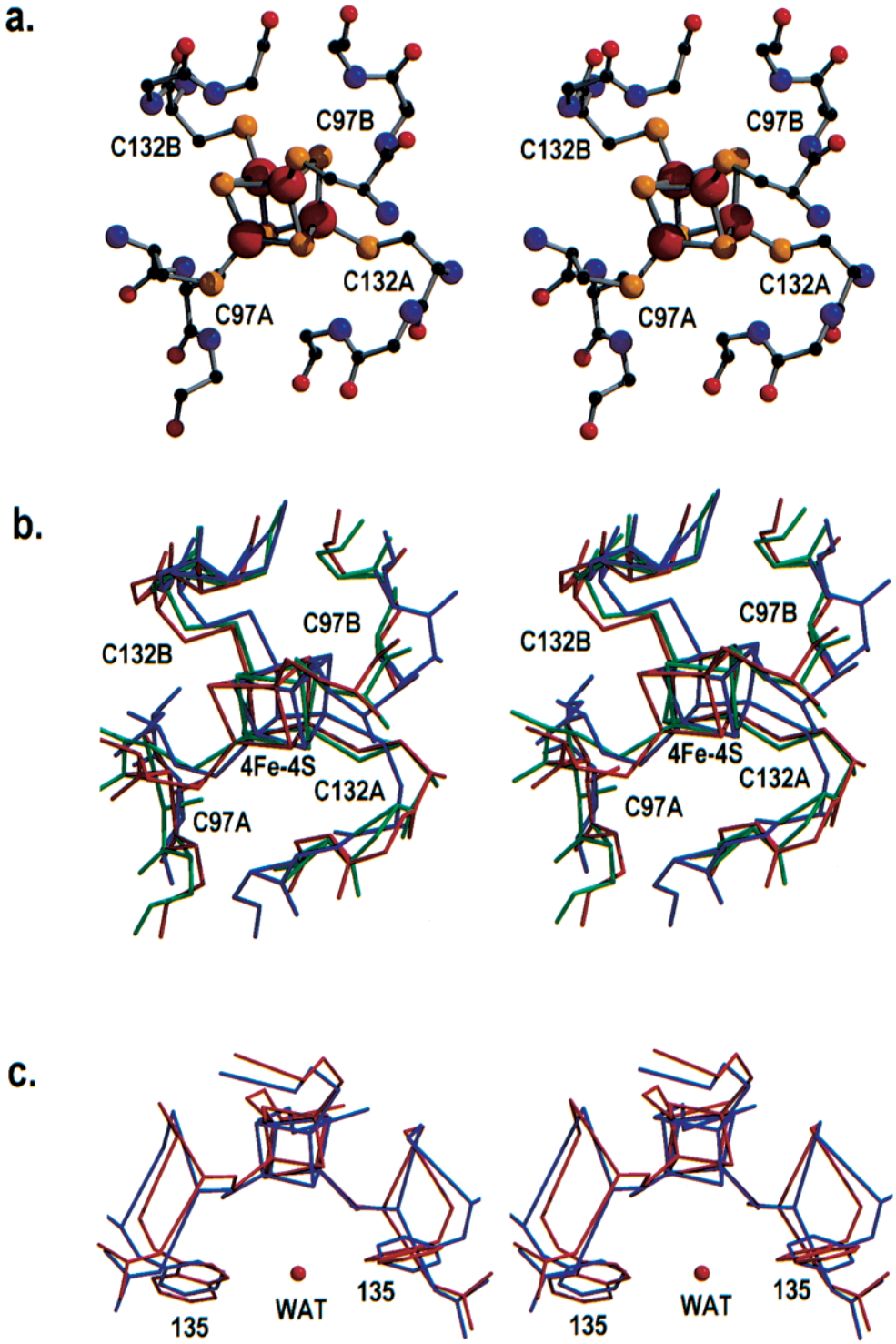


FIGURE 2: Stereoviews of (a) ball and stick diagram of the coordination environment of the [4Fe-4S] cluster of the Fe protein. The color scheme includes Fe represented in rust, S in yellow, oxygen in red, nitrogen in blue, and carbon in black. (b) Superposition of the cluster environments of native Fe protein structures 1 nip (green) and 2nip (blue) on the structure of the Trp substituted Fe protein variant (red). (c) Superposition of the structure of the native Fe protein, 1nip on the structure of the Trp substituted Fe protein variant. The relative positions of Phe and Trp in the respective structures are shown by superposition in a different view than that of panels a and b as well as the additional bound water molecule (WAT) in the Trp substituted variant structure. The native Fe protein (1nip) is shown in blue and the Trp substituted Fe protein variant is shown in red. The two subunits of the Fe protein are designated as A or B.

substituted Fe protein with that of the available native *A. vinelandii* Fe protein structures. This demands that the observed changes in the properties of the altered Fe protein [4Fe-4S] cluster must result from more localized changes.

Several factors have been shown or postulated to provide protein control of metal cluster properties in other metalloproteins. These include dipolar interactions between the protein and the metal cluster and protein control of solvent access to the metal cluster (*1*, *2*). It is not difficult to imagine that substitution at position 135, just two residues from the coordinating ligands Cys 132, could impose structural changes on the environment of the [4Fe-4S] cluster leading to the changes in the midpoint potential. A comparison of the most recent 2.2 Å native Fe protein structure (2nip) (*15*),

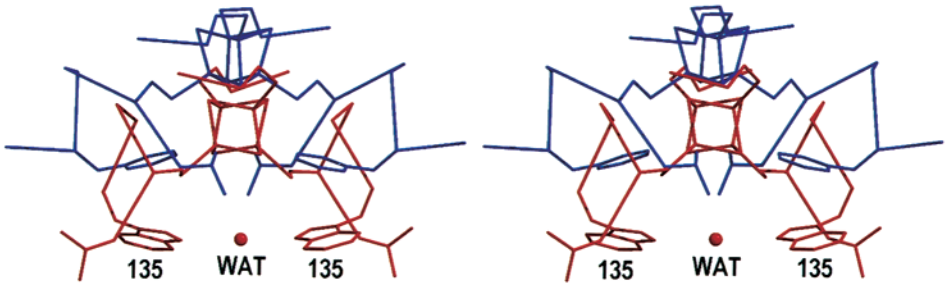


FIGURE 3: The relative position of the Phe at position 135 to the [4Fe-4S] cluster of the Fe protein from the nitrogenase Fe protein−MoFe protein complex stabilized by MgADP and tetraflouroaluminate compared to the relative position of the Trp at position 135 to the [4Fe-4S] cluster of the Trp substituted Fe protein variant. The perspective of the stereoviews is the same as that shown in Figure 2c.

Table 2: N to Cluster S Distances in the Fe Protein Structures F135W, 2nip, and 1nip and the Fe Protein from the Nitrogenase Fe Protein−MoFe Protein Complex Stabilized with MgADP and Tetraflouroaluminate[a]

| donor−acceptor | F135W (Å) | Av2 (2nip) (Å)[b] | Av2 (1nip) (Å)[c] | AlF (Å)[d] |
|---|---|---|---|---|
| C97A(N)−[4Fe-4S](S) | 4.40 | 3.80 | 3.80 | 5.10 |
| C97B(N)−[4Fe-4S](S) | 4.50 | 4.58 | 3.63 | 5.15 |
| | (4.45 ± 0.05) | (4.19 ± 0.39) | (3.72 ± 0.09) | (5.13 ± 0.03) |
| A98A(N)−[4Fe-4S](S) | 3.28 | 4.06 | 3.55 | 3.52 |
| A98B(N)−[4Fe-4S](S) | 3.39 | 3.43 | 4.02 | 3.50 |
| | (3.34 ± 0.06) | (3.75 ± 0.32) | (3.79 ± 0.24) | (3.51 ± 0.01) |
| A98A(N)−C97A(Sγ) | 3.42 | 4.06 | 2.82 | 4.19 |
| A98B(N)−C97B(Sγ) | 3.41 | 3.25 | 3.05 | 4.21 |
| | (3.42 ± 0.01) | (3.66 ± 0.41) | (2.94 ± 0.12) | (4.20 ± 0.01) |
| G99A(N)−C97A(Sγ) | 3.65 | 3.70 | 3.70 | 4.14 |
| G99B(N)−C97B(Sγ) | 3.64 | 3.38 | 3.22 | 4.14 |
| | (3.65 ± 0.01) | (3.54 ± 0.16) | (3.46 ± 0.24) | (4.14 ± 0.00) |
| G99A(N)−[4Fe-4S](S) | 4.32 | 4.57 | 5.27 | 3.01 |
| G99B(N)−[4Fe-4S](S) | 4.24 | 3.69 | 4.73 | 3.01 |
| | (4.28 ± 0.04) | (4.13 ± 0.44) | (5.00 ± 0.27) | (3.01 ± 0.00) |
| R100A(N)−C97A(Sγ) | 4.04 | 4.47 | 4.41 | 3.46 |
| R100B(N)−C97B(Sγ) | 4.05 | 4.65 | 4.46 | 3.46 |
| | (4.04 ± 0.01) | (4.56 ± 0.09) | (4.44 ± 0.03) | (3.46 ± 0.00) |
| C132A(N)−C132A(Sγ) | 3.12 | 3.16 | 2.89 | 2.87 |
| C132B(N)−C132B(Sγ) | 3.12 | 2.81 | 3.13 | 2.85 |
| | (3.12 ± 0.00) | (2.99 ± 0.17) | (3.01 ± 0.12) | (2.86 ± 0.01) |
| G133A(N)−[4Fe-4S](S) | 4.17 | 3.68 | 3.68 | 5.83 |
| G133B(N)−[4Fe-4S](S) | 4.61 | 4.09 | 4.47 | 5.81 |
| | (4.39 ± 0.22) | (3.89 ± 0.20) | (4.01 ± 0.46) | (5.82 ± 0.01) |
| G133A(N)−C132A(Sγ) | 3.85 | 4.31 | 3.30 | 4.40 |
| G133B(N)−C132B(Sγ) | 3.82 | 3.67 | 3.67 | 4.41 |
| | (3.83 ± 0.02) | (3.99 ± 0.32) | (3.49 ± 0.19) | (4.40 ± 0.01) |
| G134A(N)−C132A(Sγ) | 3.57 | 6.48 | 3.36 | 4.66 |
| G134B(N)−C132B(Sγ) | 3.64 | 3.64 | 3.85 | 4.67 |
| | (3.61 ± 0.04) | (5.06 ± 1.42) | (3.61 ± 0.24) | (4.67 ± 0.01) |
| G134A(N)−C97A(Sγ) | 4.92 | 3.58 | 6.69 | 7.84 |
| G134B(N)−C97B(Sγ) | 4.51 | 4.44 | 6.68 | 7.85 |
| | (4.72 ± 0.20) | (4.01 ± 0.43) | (6.69 ± 0.01) | (7.85 ± 0.01) |
| G134A(N)−[4Fe-4S](S) | 3.60 | 4.31 | 3.58 | 5.92 |
| G134B(N)−[4Fe-4S](S) | 3.28 | 3.67 | 3.17 | 5.95 |
| | (3.44 ± 0.16) | (3.99 ± 0.33) | (3.38 ± 0.20) | (5.93 ± 0.02) |
| F/W135A(N)−C132A(Sγ) | 3.51 | 5.24 | 3.94 | 4.83 |
| F/W135B(N)−C132B(Sγ) | 3.67 | 3.68 | 4.32 | 4.83 |
| | (3.59 ± 0.08) | (4.46 ± 0.78) | (4.13 ± 0.19) | (4.83 ± 0.00) |
| W135A(Nε)−[4Fe-4S](S) | 4.46 | NA | NA | NA |
| W135B(Nε)−[4Fe-4S](S) | 4.39 | NA | NA | NA |
| | (4.43 ± 0.04) | | | |

[a] The designation A and B denote the Fe protein subunits. [b] ref. *15*, [c] ref *9*, [d] ref *21*.

the first reported 2.8 Å native Fe protein structure (1nip) (*9*), and the Fe protein of the nitrogenase Fe protein−MoFe protein complex stabilized by tetraflouroaluminate and MgADP (*21*) indicates that there are differences in the geometry of the coordinating ligands and adjacent residues that are reflected in alternative main-chain positioning and arrangement of nearby amides. (Figure 2/Table 2). A direct comparison of the structure determined here with the most recent high-resolution structure of the native Fe protein is hampered in some cases due to apparent crystal-packing interactions that cause the cluster environment to be somewhat distorted and largely asymmetric. This asymmetry is evident in the large variation in the distances of the amide N atoms to S atoms in the environment of the [4Fe-4S] cluster when comparing corresponding interactions in the Fe protein monomers related by noncrystallographic symmetry (NCS) (*15*) (Table 2). However, there are some variations in the distances of the amide N atoms to S atoms in

comparing NCS-related monomers, albeit to a lesser extent, in the original 2.8 Å native Fe protein structure (1nip) and the structure of the Trp-substituted Fe protein variant. This variability may also arise from crystal lattice contacts; however, since the structure of the Trp-substituted Fe protein variant was determined in the same monoclinic space group symmetry with similar cell parameters as the native Fe protein (*9*), 1nip, comparisons are much easier. This variation between NCS-related monomers is not observed in the Fe protein of the nitrogenase complex stabilized by tetraflouroaluminate and MgADP where strict NCS constraints were applied (*21*). The amides shown in the table are indicated on the basis of distance only without regard to directional geometry with respect to productive hydrogen bond formation since the presence of these amides irrespective of orientation would contribute to the local charge of the cluster and to the apparent midpoint potential due to microsolvation effects. An important observation is that the amides in the environment (Table 2/Figure 2) are located at N termini of α-helices that terminate at the Cys cluster ligands and could therefore have a significantly stronger dipole moment than a single uncoupled dipole. The individual helix dipoles could account for a larger charge and significantly larger dipole moment such that the amide N atoms at their termini would approach a formal positive charge. This could be a significant factor in stabilizing the reduced state of the cluster consistent with the more negative midpoint potential that has been observed for the [4Fe-4S] cluster of the Fe protein within this complex (*28*). Additionally, although the differences are subtle, these helices appear to be directed to a slightly greater extent in the structure of the Trp-substituted Fe protein variant.

The trends of the distances shown here indicate that the positions of these amide N atoms are variable in the structures. These trends indicate that several of the amide nitrogens are different in a manner that is consistent with the observed differences in midpoint potentials. For example, comparing the native Fe protein with the Fe protein in the tetraflouroaluminate/MgADP-stabilized nitrogenase complex, although a few N−S distances decrease, the majority of the N−S distances that change are observed to be longer in the complex than in the native Fe protein (Table 2), and it is known that in the complex the midpoint potential is significantly negatively shifted (*28*). It is conceivable that the observed changes in midpoint potential are due, primarily, to a combination of the proximity of the individual amide N atoms and the overall orientation of the helix dipoles that are located adjacent to the [4Fe-4S] cluster and terminate in the cluster ligands. These changes could contribute to the observed more positive midpoint potential observed in Trp substituted Fe protein variant.

Another factor worth considering in modulating the midpoint potential of the [4Fe-4S] cluster of the Fe protein is bulk solvent accessibility. In much the same manner as the aforementioned interaction of the single ordered solvent molecule, bulk solvent accessibility is thought to impact the midpoint potential due to the dipolar character of individual solvent atoms (*1*, *2*). Increased solvent accessibility should stabilize the reduced state of the cluster and favor a cluster with a more positive midpoint potential. If again we consider the conformational changes observed in the nitrogenase complex stabilized with MgADP and tetraflouroaluminate as a crude approximation of the conformational changes observed in the MoFe protein independent MgATP bound form of the Fe protein, then the solvent accessibility of the cluster would be increased (*15*, *21*). Therefore, if solvent accessibility is a dominating factor, then it would be expected that the MoFe protein independent form of the Fe protein would have a more positive midpoint potential. MgATP binding to the Fe protein results in a negative shift in the midpoint potential, suggesting that solvent accessibility is unlikely to be a dominating factor.

*Nucleotide Interactions.* In the presence of MgADP or MgATP, the Fe protein undergoes conformational changes that result in changes in the midpoint potential (*25*−*28*) and spectroscopic properties (*25*, *29*−*33*) of the [4Fe-4S] cluster. In addition, the [4Fe-4S] cluster of the MgATP-bound form of the Fe protein becomes more susceptible to specific metal chelators (*55*, *56*). It is generally thought that the conformational changes result in a rigid body reorientation of the Fe protein monomers with respect to one another closing the dimer interface. This rigid body reorientation is observed in the nitrogenase Fe protein−MoFe protein complex stabilized with tetraflouroaluminate and MgADP (*21*). The results of small-angle X-ray-scattering studies are also in support of a similar rigid body reorientation of the monomers in the presence of MgATP but in the absence of the MoFe protein (*57*). These conformational changes are critical to the productive interaction of the Fe protein with the MoFe protein in order to bring about MgATP hydrolysis and electron transfer to substrates (*3*, *4*, *6*). Upon nucleotide binding, the Trp-substituted Fe protein variant appears to undergo nucleotide-dependent conformational changes exhibited by specific spectroscopic changes, susceptibility of the [4Fe-4S] cluster to chelators, and specific shifts in the midpoint potential of the [4Fe-4S] cluster (*39*). The observed shifts in the midpoint potential could result from the repositioning of the cluster adjacent helix dipoles as mentioned above. Interestingly, the Trp-substituted Fe protein variant is unable to productively interact with the MoFe protein or bring about MgATP hydrolysis or electron transfer. Examination of the structure of the Trp-substituted variant indicates that the regions of the Fe protein presumed to be involved in nucleotide interactions appear to be unaffected by the substitution. Of course, it is impossible to say whether these interactions may be altered in an MgATP-bound state; however, the Trp-substituted variant exhibits similar affinities for MgADP and MgATP. A more straightforward interpretation of the inability of this Fe protein to act in catalysis is the inability of the Fe protein variant to achieve the extent of conformational changes necessary for a productive interaction with the MoFe protein. Although conformational changes are undoubtedly imposed on the MgATP-bound Fe protein upon interaction with the MoFe protein, it is generally thought that the conformational changes brought about by MgATP binding alone are along the lines of those observed in the nitrogenase complex. Extrapolation of the conformation changes observed in the Fe protein when complexed with the MoFe protein in the MgADP and tetraflouroaluminate-stabilized complex (*21*) on the Trp-substituted Fe protein variant suggests that the bulkier Trp group would prevent the extent of comformational changes observed in the complex (Figure 3). In the nitrogenase complex Phe 135 is involved in a tightly packed group of hydrophobic residues

located at the face of the [4Fe-4S] cluster distal to the Fe protein−MoFe protein docking interface. The above extrapolation also would suggest that the amide N of Trp would approach the cluster even more closely than in the nucleotide-free state observed, which would be consistent with a positive shift in the midpoint potential upon MgATP binding. This is counter to the previous observations that indicate a negative shift in the midpoint potential upon MgATP binding to the Trp-substituted variant (*39*). This may indicate that this type of extrapolation does not mimic the specific changes brought about by the binding of nucleotide alone or the contributions of the orientation and distance of the helix dipoles are much more significant in modulating the midpoint potential of the [4Fe-4S] cluster of the Fe protein.

## CONCLUSIONS

Although the aromatic character of Phe at position 135 has been retained, the structure of the Trp 135 variant demonstrates specific changes in the environment of the [4Fe-4S] cluster. The most notable of these changes that could contribute to the specific modulation of the midpoint potential of the [4Fe-4S] include: first, the introduction of the Trp indole amide located ∼4.4 Å from the cluster inorganic S atoms; second, the presence of a bound water molecule located between the Trp indole amides and also in close proximity to the cluster inorganic S atoms; and third, specific changes in the location of peptide bond amide nitrogens, specifically the repositioning of the amide of the substituted Trp to come to within ∼3.6 Å of a cluster inorganic sulfur atom.

The culmination of the structure of the Trp-substituted Fe protein variant together with detailed comparisons of the available Fe protein structures has lead to a reevaluation of the factors which dictate the changes in midpoint potentials of the [4Fe-4S] cluster upon nucleotide binding and complex formation. Conformational changes that drive the orientation and proximity of dipoles with respect to the [4Fe-4S] cluster of the Fe protein presents an elegant mechanism by which large changes in the midpoint potential can be modulated.

## ACKNOWLEDGMENT

We thank Jeannine Chan and Dr. Jennifer Huyett of Utah State University for assistance in enzyme purification.

## REFERENCES

1. Langen, R., Jensen, G. M., Jacob, U., Stephens, P. J., and Warshel, A. (1992) *J. Biol. Chem. 267*, 25625−25627.
2. Stephens, P. J., Jollie, D. R., and Warshel, A. (1996) *Chem. Rev. 96*, 2491−2513.
3. Peters, J. W., Fisher, K., and Dean, D. R. (1995) *Annu. Rev. Microbiol. 49*, 335−366.
4. Burgess, B. K., and Lowe, D. J. (1996) *Chem. Rev. 96*, 2983−3011.
5. Eady, R. R. (1996) *Chem. Rev. 96*, 3013−3030.
6. Howard, J. B., and Rees, D. C. (1996) *Chem. Rev. 96*, 2965−2982.
7. Thorneley, R. N. F., and Lowe, D. J. (1996) *J. Biol. Inorg. Chem. 1*, 576−580.
8. Seefeldt, L. C., and Dean, D. R. (1997) *Acc. Chem. Res. 30*, 260−266.
9. Georgiadis, M. M., Komiya, H., Chakrabarti, P., Woo, D., Kornuc, J. J., and Rees, D. C. (1992) *Science 257*, 1653−1659.
10. Kim, J., and Rees, D. C. (1992) *Science 257*, 1677−1682.
11. Kim, J., and Rees, D. C. (1992) *Nature 360*, 553−560.
12. Bolin, J. T., Campobasso, N., Muchmore, S. W., Morgan, T. V., and Mortenson, L. E. (1993) in *Molybdenum Enzymes, Cofactors and Model Systems* (Stiefel, E. I., Coucouvanis, D., and Newton, W. E., Eds.) pp 186−195, American Chemical Society, Washington DC.
13. Chan, M. K., Kim, J., and Rees, D. C. (1993) *Science 260*, 792−794.
14. Kim, J., Woo, D., and Rees, D. C. (1993) *Biochemistry 32*, 7104−7115.
15. Schlessman, J. L., Woo, D., Joshua-Tor, L., Howard, J. B., and Rees, D. C. (1998) *J. Mol. Biol. 280*, 669−685.
16. Shah, V. K., and Brill, W. J. (1977) *Proc. Natl. Acad. Sci. U.S.A. 74*, 3249−3253.
17. Lowe, D. J., Fisher, K., and Thorneley, R. N. F. (1993) *Biochem. J. 292*, 93−98.
18. Peters, J. W., Fisher, K., Newton, W. E., and Dean, D. R. (1995) *J. Biol. Chem. 270*, 27007−27013.
19. Lanzilotta, W. N., and Seefeldt, L. C. (1996) *Biochemistry 35*, 16770−16776.
20. Angove, H., Yoo, S. J., Munck, E., and Burgess, B. K. (1998) *J. Biol. Chem. 273*, 26330−26337.
21. Schindelin, H., Kisker, C., Schlessman, J. L., Howard, J. B., and Rees, D. C. (1997) *Nature 387*, 370−376.
22. Hageman, R. V., and Burris, R. H. (1978) *Proc. Natl. Acad. Sci. U.S.A. 75*, 2699−2702.
23. Shultz, G. E. (1992) *Curr. Opin. Struct. Biol. 2*, 61−67.
24. Koonin, E. V. (1993) *J. Mol. Biol. 229*, 1165−1174.
25. Zumft, W. G., Palmer, G., and Mortenson, L. E. (1973) *Biochim. Biophys. Acta 292*, 413−421.
26. Watt, G. D., Wang, Z. C., and Knotts, R. R. (1986) *Biochemistry 25*, 8156−8162.
27. Lanzilotta, W. N., and Seefeldt, L. C. (1997) *Biochemistry 36*, 12976−12983.
28. Spee, J. H., Arendsen, A. F., Wassink, H., Marritt, S. J., Hagen, W. R., and Haaker, H. (1998) *FEBS Lett. 432*, 55−58.
29. Stephens, P. J., McKenna, C. E., Smith, B. E., Nguyen, H. T., McKenna, M. C., Thomson, A. J., Devlin, F., and Jones, J. B. (1979) *Proc. Natl. Acad. Sci. U.S.A. 76*, 2585−2589.
30. Lindahl, P. A., Gorelick, N. J., Münck, E., and Orme-Johnson, W. H. (1987) *J. Biol. Chem. 262*, 14945−14953.
31. Meyer, J., Gaillard, J., and Moulis, J. M. (1988) *Biochemistry 27*, 6150−6156.
32. Lanzilotta, W. N., Holz, R. C., and Seefeldt, L. C. (1995) *Biochemistry 34*, 15646−15653.
33. Ryle, M. J., Lanzilotta, W. N., Seefeldt, L. C., Scarrow, R. C., and Jensen, G. M. (1996) *J. Biol. Chem. 271*, 1551−1557.
34. Carter, C. W. Jr., Kraut, J., Freer, S. T., Xuong, N. H., Alden, R. A., and Bartsch, R. G. (1974) *J. Biol. Chem. 249*, 4212−4225.
35. Adman, E., Watenpaugh, K. D., and Jensen, L. H. (1975) *Proc. Natl. Acad. Sci. U.S.A. 72*, 4854−4858.
36. Breiter, D. R., Meyer, T. E., Rayment, I., and Holden, H. M. (1991) *J. Biol. Chem. 266*, 18660−18667.
37. Jensen, G. M., Warshel, A., and Stephens, P. J. (1994) *Biochemistry 33*, 10911−10924.
38. Heering, H. A., Bulsink, Y. B. M., Hagen, W. R., and Meyer, T. E. (1995) *Eur. J. Biochem. 232*, 811−817.
39. Ryle, M. J., Lanzilotta, W. N., and Seefeldt, L. C. (1996) *Biochemistry 35*, 9424−9434.
40. Chromy, V., Fischer, J., and Kulhanek, V. (1974) *Clin. Chem. 20*, 1362−1363.
41. Hathaway, G. M., Lundak, T. S., Tahara, S. M., and Traugh, J. A. (1979) *Methods Enzymol. 60*, 495−511.
42. Otwinowski, Z. (1991) *Data Collection and Processing*, SERC Daresbury Laboratory, Daresbury, U.K.
43. Navaza, J. (1994) *Acta Crystallogr., Sect. D 50*, 1507−1516.
44. Abrahams, J. P., and Leslie, A. (1996) *Acta Crystallogr., Sect. D 52*, 30−42.
45. Jones, T. A., Zou, J. Y., Cowan, S. W., and Kjeldgaard. (1991) *Acta Crystallogr, Sect. A 47*, 110−119.

46. Brunger, A. T. (1992) *Nature 355*, 472−475.
47. Brunger, A. T. (1992) *X-PLOR version 3.1 − A system for X-ray crystallography and NMR*, Yale University Press, New Haven and London.
48. Kabsch, W. (1976) *Acta Crystallogr., Sect. A 32*, 922−923.
49. Laskowski, R. A., McArthur, M. W., Moss, D. S., and Thornton, J. M. (1993) *J. Appl. Crystallogr. 26*, 283−291.
50. Kraulis, P. J. (1991) *J. Appl. Crystallogr. 24*, 946−950.
51. Esnouf, R. M. (1997) *J. Mol. Graphics 15*, 133−138.
52. Merritt, E. A., and Murphy, M. E. P. (1994) *Acta Crystallogr., Sect. D 50*, 869−873.
53. Wolle, D., Dean, D. R., and Howard, J. B. (1992) *Science 258*, 992−995.
54. Ryle, M. J., and Seefeldt, L. C. (1996) *Biochemistry 35*, 4766−4775.
55. Walker, G. A., and Mortenson, L. E. (1974) *Biochemistry 13*, 2382−2388.
56. Ljones, T., and Burris, R. H. (1978) *Biochemistry 17*, 1866−1872.
57. Chen, L., Gavini, N., Tsuruta, H., Eliezer, D., Burgess, B. K., Doniach, S., and Hodgson, K. O. (1994) *J. Biol. Chem. 269*, 3290−3294.

BI991694V